ACS Sustainable Chemistry & Engineering

Research Article

pubs.acs.org/journal/ascecg

# Facile Preparation of Monodisperse Carbon Spheres: Template-Free Construction and Their Hydrogen Storage Properties

Jiafu Chen, Zhanlin Lang, Qun Xu,* Bo Hu, Jianwei Fu, Zhimin Chen, and Jianan Zhang

College of Materials Science and Engineering, Zhengzhou University, Zhengzhou 450052, P.R. China

Supporting Information

**ABSTRACT:** A simple and effective template-free method to prepare monodisperse carbon spheres has been successfully developed using solid poly(styrene-co-divinylbenzene) (P(St-co-DVB)) nanospheres as the raw material, anhydrous aluminum chloride as the Friedel–Crafts catalyst, and carbon tetrachloride as a cross-linker and solvent. The pore structure in the spheres can be tailored by substituting hollow P(St-co-DVB) capsules (HPCs) for solid P(St-co-DVB) spheres (SPSs). Experimental results show that the micropore size of the spheres obtained from HPCs increases compared to that of the spheres obtained from SPSs, and the pore volume and the specific surface area also have changed. The mechanism behind these phenomena and the hydrogen storage properties of the obtained carbon spheres at 77 K and 1 atm are further studied in this work.

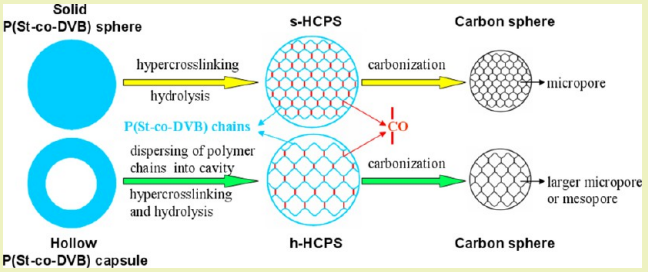


**KEYWORDS:** *Monodisperse carbon spheres, Template-free construction, Pore structure, Hydrogen storage*

## INTRODUCTION

Over the past few years, increasing attention has been paid to porous carbons with designed pore architecture[1] because they can be used as an effective sorbent,[2] catalyst support,[3,4] filter,[5] and electrode for a range of applications.[6−8] These applications require that the porous carbon materials have special internal morphology (ordered or disordered micro-, meso-, or macropores). Usually, porous carbons with large pore volumes are suitable for sensor substrates. As a glucose sensor, a mesoporous carbon foam (MSU-F-C) is used as an immobilization host for glucose oxidase due to the large pores of MSU-F-C.[7] As an electrochemical double-layer capacitor electrode material, it is necessary for porous carbon to have an interconnected porous network with sufficiently open mesopore windows for electrolyte wetting and rapid ionic transportation.[1,8] Porous carbons with micropore structure are suitable for hydrogen physisorption because smaller pores produce the stronger C−$H_2$ interaction and increase both the heat of adsorption and total volume of adsorbed hydrogen.[9] The optimal pore size for hydrogen adsorption is 0.65−0.9 nm in the porous carbon.[10] Therefore, construction of micropores and tuning of the pore size distribution (PSD) with sub-angstrom accuracy in the porous carbon are necessary for the purpose to optimize porous carbon and enhance hydrogen uptake capacity.[11,12]

Most of the porous carbons are prepared by templating methods.[13−18] The porous structure of the obtained carbon materials is determined by the type of inorganic template used, which allows precise control of the porous structure of carbons.[13,14] Usually, the pore size and porosity of the micro- or mesoporous carbons are further varied beneficially by physical or chemical activation.[15−18] However, these referred methods have some inevitable limitations, for instance, the procedure is tedious due to fabrication of templates of special nanostructures, removal of hard templates, and/or post activation treatment, etc.[19] Therefore, a simple and effective route to form micropores and tune PSD with sub-angstrom accuracy in the porous carbons remains a challenge.

Considering the limitations mentioned above, a simple and effective template-free method to form micropores in monodisperse carbon spheres has been successfully developed in this work. The micropore structure in the spheres can be tailored by substituting hollow P(St-co-DVB) capsules (HPCs) for solid P(St-co-DVB) spheres (SPSs). This method avoids the use of any hard-/soft-templates, thereby endowing the as-prepared porous spheres with a very competitive price-to-performance ratio using low-cost styrenic polymers as carbon resources. In addition, the mechanism behind these phenomena has been studied. Such a mechanism of tailoring pore structure enriches the tailoring theories of pore texture, and the hydrogen storage properties of the obtained carbon spheres at 77 K and 1 atm are also obtained.

## EXPERIMENTAL SECTION

**Preparation of SPSs and HPCs.** The monodisperse SPSs with core–shell structure were synthesized by soap-free emulsion polymerization that was carried out in a four-necked flask (250 mL) in a thermostatted water bath. In a typical polymerization, 2.1 g of styrene

Received: April 27, 2013
Revised: May 19, 2013
Published: May 24, 2013

  

(St) and 90 g of deionized water were added into the flask. The solution was vigorously stirred at a speed of 200 rpm, while it was deoxygenated by bubbling nitrogen. Thirty minutes later, the solution began to heat up. After the temperature rose to 70 °C, 10 mL of aqueous solution containing 0.12 g of potassium persulfate (KPS) was added into the flask, and this moment was regarded as the start time of the polymerization. The obtained SPSs containing 35 and 40 wt % DVB were, respectively, labeled as SPSs-35 and SPSs-40. The detailed recipes are listed in Table S1 of the Supporting Information.

A total of 0.24 g of SPSs was put into tetrachloromethane ($CCl_4$) (24 mL) in a three-necked flask in a thermostatted water bath, and the mixture was vigorously stirred at a speed of 160 rpm at 40 °C. Ten hours later, the product was collected and purified by centrifugation and redispersion in acetone by ultrasonic. These HPCs obtained from SPSs-35 and SPSs-40 were, respectively, labeled as HPCs-35 and HPCs-40.

**Preparation and Carbonization of Hypercrosslinked Polystyrene Spheres (HCPSs).** The hypercrosslinking reaction was conducted in a three-necked flask (125 mL) equipped with a polytetrafluoroethylene-bladed paddle stirrer and a water-cooled reflux condenser. In a typical reaction, 30 mL of $CCl_4$ and 1.80 g of anhydrous aluminum trichloride ($AlCl_3$) were put into the flask, and the solution was vigorously stirred at room temperature. Twenty minutes later, 0.30 g of SPSs or HPCs was added into the solution. Forty minutes later, the flask was put into a water bath of 60 °C, and this moment was regarded as the start time of the reaction. After the reaction lasted 16 h, the product was collected and purified by centrifugation and redispersion in acetone by ultrasonic, and then it was washed with dilute hydrochloric acid three times. The obtained solid product was collected and dried at 45 °C. The final hypercrosslinked products obtained were labeled as s-HCPSs-35, s-HCPSs-40, h-HCPSs-35, and h-HCPSs-40, respectively.

Carbonization of HCPSs was carried out in a tube furnace in the nitrogen atmosphere. The carbonization temperature was elevated homogeneously to 700 °C and then was held at 700 °C for 2 h under a nitrogen flow. The product was collected after it was naturally cooled to room temperature under a nitrogen flow. The final products obtained from s-HCPSs-35, s-HCPSs-40, h-HCPSs-35, and h-HCPSs-40 were, respectively, labeled as CS35, CS40, CH35, and CH40. Besides, the final product obtained by carbonizing s-HCPSs-35 at 900 °C was labeled as CS35-900.

**Characterization.** Fourier transform infrared (FT-IR) spectra were measured in the wavenumber range from 4000 to 400 $cm^{-1}$ by using a Bruker Optics TENSOR 27 FT-IR spectrophotometer. X-ray diffraction (XRD) was carried out on a Y-2000 X-ray diffractometer with Cu K$\alpha$ radiation ($\lambda$ = 0.15406 nm) operating at 40 kV and 40 mA. Raman spectra were obtained at 514.5 nm laser excitation on a Renishaw microscope system RM2000 at room temperature. The laser power density was kept less than 3 mW with a resolution of 1.5−2.0 $cm^{-1}$ over the spectral window. Spectra were collected at various locations on each sample studied to determine the reproducibility. The morphologies and structures of the samples were investigated with a FEI Quanta 200 scanning electron microscope (SEM) and a FEI Tecnai G2 20 transmission electron microscope (TEM) with an accelerating voltage of 120 kV. Nitrogen adsorption/desorption measurements were performed in a Micromeritics ASAP 2020 instrument at 77 K. The micropore volume and size distribution were, respectively, calculated by the Dubinin−Radushkevich (DR) equation and Horvath−Kawazoe (HK) method. The total pore volume was calculated at a relative pressure $P/P_0$ = 0.99. Hydrogen uptake capacities were tested volumetrically. Volumetric approach was performed on the Micrometrics ASAP 2020 instrument. The samples were degassed at 300 °C under vacuum overnight, and hydrogen was adsorbed over the range of 0−775 mmHg at 77 K.

## RESULTS AND DISCUSSION

Figure 1 shows TEM photos of the typical HPCs and h-HCPSs with 40 wt %. HPCs-40 are prepared by dissolving cores of SPSs with 40 wt % DVB using $CCl_4$ at 40 °C,[20] and h-HCPSs-40 are prepared by hypercrosslinking of HPCs-40 at 60 °C using $CCl_4$ as a cross-linker and solvent. The TEM results show that the h-HCPSs-40 have a solid homogeneous structure and the same diameter (about 320 nm) with HPCs-40. This phenomenon could be explained by the following. At the beginning of the hypercrosslinking reaction, the HPCs are swelled in $CCl_4$ and form intact spherical shapes. The P(St-co-DVB) chains in the exterior of the HPCs are first cross-linked by $CCl_4$ and form cross-linked networks. The cross-linked networks prevent the P(St-co-DVB) chains in the HPCs, which are dissolved by $CCl_4$ at 60 °C and not dissolved at 40 °C. As a result, the P(St-co-DVB) chains in the HPCs are only dispersed and transferred into their cavities and are subsequently cross-linked by $CCl_4$, finally forming solid homogeneous h-HCPSs (Figure 1b). Because of the same dimension of HPCs-40 and h-HCPSs-40, there was no volume change for the hollow P(St-co-DVB) spheres during the hypercrosslinking reaction. It can be suggested that much larger interspaces among the polymer chains can be produced in h-HCPS-40 than s-HCPSs-40.

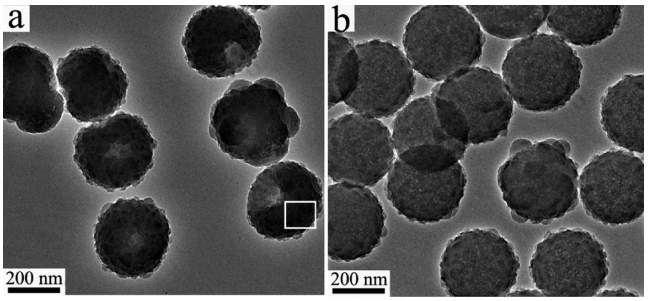


**Figure 1.** TEM photos of the typical HPCs and h-HCPSs with 40 wt % DVB. (a) HPCs-40 and (b) h-HCPSs-40.

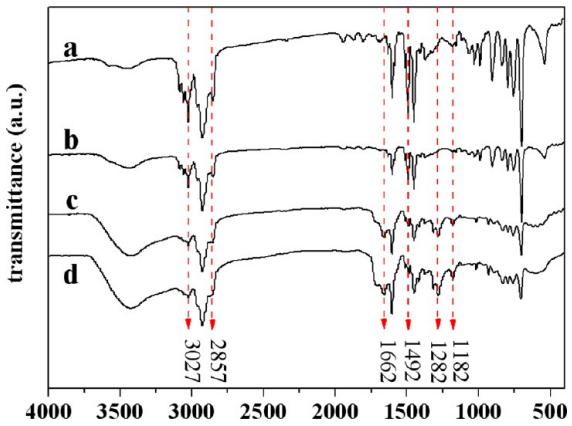


**Figure 2.** FT-IR spectra of the typical samples with 35 wt % DVB. (a) SPSs-35, (b) HPCs-35, (c) s-HCPSs-35, and (d) h-HCPSs-35.

FT-IR spectra of the typical samples with 35 wt % DVB are shown in Figure 2. The peak at 3400−3500 $cm^{-1}$ was ascribed to the O−H stretching vibration of $H_2O$, which was from KBr during the FT-IR measurement. The peaks between 3100 and 2800 $cm^{-1}$ were ascribed to the stretching vibrations of C−H and $-CH_2-$ of the polystyrene (PS), and the peaks between 1500 and 1400 $cm^{-1}$ were ascribed to C−H bending vibrations.[21] After the hypercrosslinking reaction using $CCl_4$ as a cross-linker, the relative intensity of the peaks at 3027, 2857, and 1492 $cm^{-1}$ distinctly weakens, and the peaks at 1282 and 1182 $cm^{-1}$ ascribed to C−Cl bending vibration appear (Figure 2c,d), which demonstrate the occurrence of Friedel−

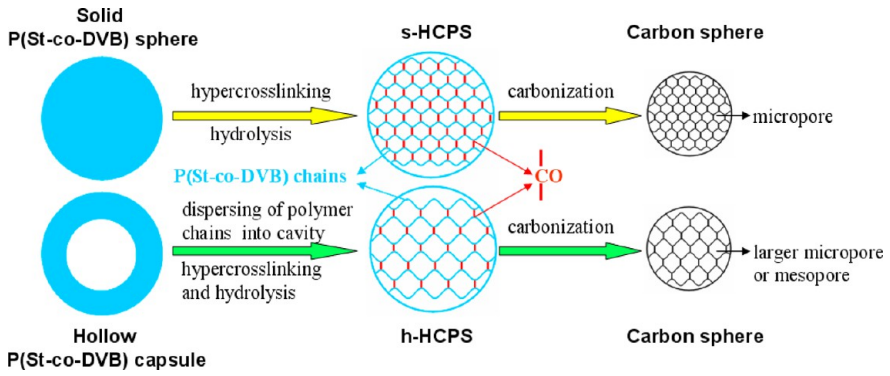


**Figure 3.** Illustration of the template-free routes to construct various pore structures of the carbon spheres using solid P(St-co-DVB) spheres (SPSs) or hollow P(St-co-DVB) capsules (HPCs) as the raw materials.

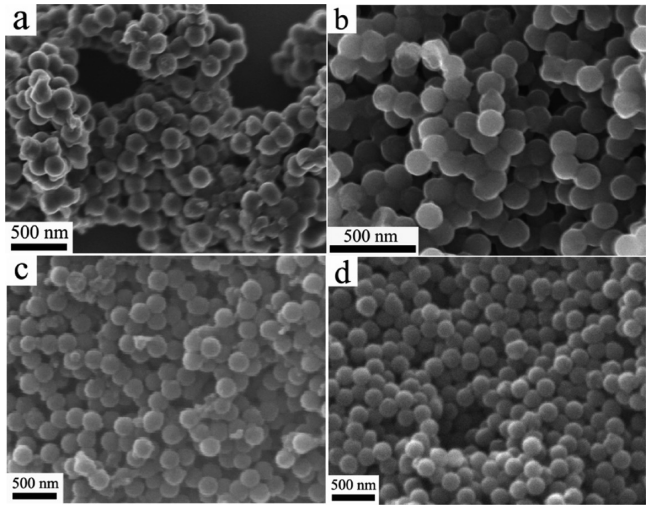


**Figure 4.** SEM photos of the carbon spheres prepared using SPSs and HPCs as the raw materials. (a) CS35, (b) CH35, (c) CS40, and (d) CH40.

Crafts alkylation.[22,23] The obvious peak at 1662 $cm^{-1}$ is ascribed to stretching of the C═O band coming from the constructed carbonyl (−CO−) cross-linking bridges, which are produced by the hydrolyzation of the $-CCl_2-$ cross-linking bridges between phenyl rings during washing and drying due to the presence of $H_2O$ after the Friedel−Crafts reaction.[24] The constructed −CO− cross-linking bridges provide a high cross-linking density and a proper amount of oxygen atoms, achieving good framework carbonizability and nanostructure inheritability during carbonization of s-HCPSs and h-HCPSs.[19]

In the hypercrosslinking process, the P(St-co-DVB) chains in the shells of HPCs can be dispersed and transferred into their cavities, and much larger interspaces among the P(St-co-DVB) chains can be produced in h-HCPSs than s-HCPSs. These will contribute to the final texture of the spheres after their carbonization. Hereby, two template-free routes to construct various pore structures of the carbon spheres using SPSs or HPCs as the raw materials are introduced and illustrated in Figure 3. One is hypercrosslinking the SPSs and then carbonizing s-HCPSs to obtain microporous spheres (yellow route in Figure 3). The second route is hypercrosslinking the HPCs fabricated from the SPSs[20] and then carbonizing h-HCPSs to obtain spheres with larger micropores or mesopores (green route in Figure 3).

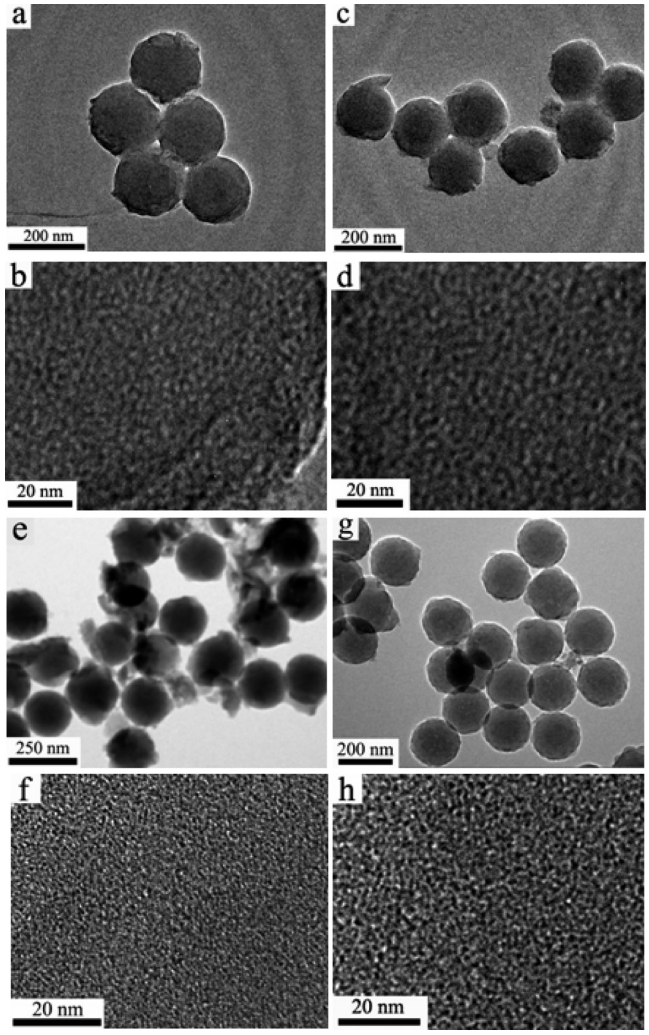


**Figure 5.** TEM photos of the carbon spheres prepared using SPSs and HPCs as the raw materials. (a,b) CS35, (c,d) CH35 (e,f) CS40, and (g,h) CH40.

SEM photos of the carbon spheres, which are prepared using SPSs and HPCs as the raw materials, are shown in Figure 4. The spheres obtained from SPSs-35, HPCs-35, SPSs-40, and HPCs-40 are, respectively, labeled as CS35, CH35, CS40, and CH40. Their TEM photos are shown in Figure 5. It can be observed that the obtained spheres are all solid spheres, and large amounts of micropores and worm-like channels are

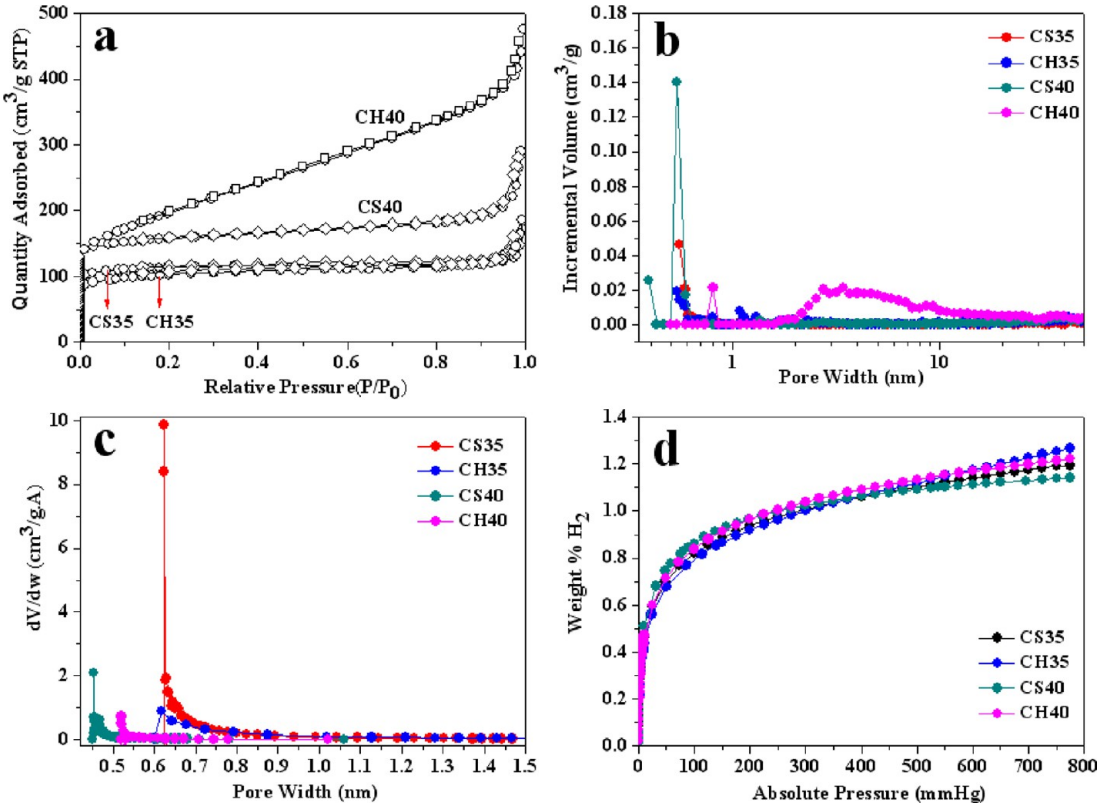


**Figure 6.** (a) Nitrogen adsorption/desorption isotherms of the obtained carbon spheres. (b) PSD derived from the DFT method. (c) Micropore size distributions analyzed by the HK method. (d) Hydrogen adsorption isotherms at 77 K under pressure up to 775 mmHg.

**Table 1. PSD Regions Obtained by DFT Method and HK Method**

| samples | PSD−DFT (nm) | PSD−HK (nm) |
|---|---|---|
| CS35 | 0.54−0.87, 1.05−2.59, >12.4 | 0.62−1.18 |
| CH35 | 0.54−0.83, 1.05−1.50, 1.55−3.89, >12.4 | 0.60−1.26 |
| CS40 | 0.39−0.43, 0.50−0.64, >7.18 | 0.45−0.61 |
| CH40 | 0.73−0.86, >1.60 | 0.52−0.63 |

**Table 2. Textural Parameters and Hydrogen Storage Capacities of Carbon Spheres**

| samples | $S_{BET}$[a] ($m^2$/g) | $V_t$[b] ($m^3$/g) | $V_{micro}$[c] ($cm^3$/g) | $V_{micro}/V_t$ (%) | $D_{HK}$[d] (nm) | $H_2$ uptake per SSA[e] |
|---|---|---|---|---|---|---|
| CS35 | 385 | 0.20 | 0.17 | 85 | 0.68 | 3.1 |
| CH35 | 350 | 0.21 | 0.15 | 71 | 0.72 | 3.6 |
| CS40 | 485 | 0.45 | 0.23 | 51 | 0.49 | 2.4 |
| CH40 | 679 | 0.74 | 0.24 | 32 | 0.52 | 1.8 |

[a]Specific surface area (SSA) calculated by the Brunauer−Emmett−Teller (BET) method. [b]Total pore volume. [c]Microporous volume determined by the DR analysis. [d]Median micropore size calculated by the HK method. [e]$H_2$ uptake per SSA calculated by $[(\text{wt \% g})/(\text{m}^2)] \times 10^3$ (ref 12).

homogeneously dispersed in the carbon matrix. It is noticeable that according to the high resolution phases of CS40 and CH40 (Figure 5 f,h), the pore sizes in CH40 are apparently larger than those in CS40. This should be ascribed to the larger interspaces among the polymer chains in h-HCPSs-40 than s-HCPSs-40 and a high cross-linking density provided by the −CO− cross-linking bridges.

Nitrogen adsorption/desorption isotherms of the obtained carbon spheres are shown in Figure 6a. Their isotherms belong to type I. The nitrogen adsorbed below $P/P_0$ of 0.02 is due to the filling of micropores, and the uptake from 0.02 to 0.2 may be ascribed to the presence of ultramicropores and small mesopores.[25] Large quantity of nitrogen could be adsorbed under the relative pressure range ($P/P_0$) lower than 0.02, which indicates the presence of a lot of micropores. A well-defined knee and an almost horizontal section between relative pressures of 0.1−0.9 indicate a monomodal distribution of micropores. For the CH40 sample, the increase in nitrogen adsorption in the relative pressure range of 0.03−0.95 should be ascribed to the presence of mesopores. In addition, the significant increase in adsorption quantity at $P/P_0 > 0.95$ is most probably due to the interstitial spaces among the spheres.

PSD curves derived from the density function theory (DFT) method are shown in Figure 6b. Because of slow diffusion and pore connectivity, the $N_2$ adsorption isotherm might not be completely equilibrated, which results in the shifting of the isotherm to higher pressures. Therefore, $N_2$ at its boiling point might be less sensitive to ultramicropores in DFT calculations.[26] Further, micropore size distribution curves derived from the HK method are shown in Figure 6c. The detailed regions of micro- and mesopore size that could be observed in the PSD curves (Figure 6 b,c) are listed in Table 1, and the textural parameters of the obtained carbon spheres are summarized in Table 2. Two regions of ultramicropores with size of 0.39−0.43 nm and 0.50−0.64 nm could be observed for the CS40 sample. As for the CH40 sample, two regions are also observed: one region is micropores with size of 0.73−0.86 nm, the other is micropores and mesopores of >1.6 nm. Compared with the CS40 sample, the increase in micropore size and $V_t$ of the CH40 sample is attributed to larger interspaces produced by reframing of polymer chains in h-HCPSs-40 and a high

cross-linking density provided by the −CO− cross-linking bridges among the P(St-co-DVB) chains. Besides, micropore size distributions analyzed by the HK method also show that the micropore size of CH40 (0.52−0.63 nm) is larger than that of CS40 (0.45−0.61 nm), and the $D_{HK}$ (0.52 nm) of CH40 is larger than that (0.49 nm) of CS40. Similar results appear in the CS35 and CH35. It is concluded that the micropore size of the spheres could be tuned with sub-angstrom accuracy by selective carbonizing h-HCPSs and s-HCPSs obtained from HPCs and SPSs with different DVB dosage, and their pore volume and specific surface area (SSA) are adjusted.

Hydrogen sorption isotherms of the carbon spheres are plotted in Figure 6d, and their hydrogen storage capacities at 77 K and 1 atm are summarized in Table 2. For carbonaceous adsorbents, the optimal pore size is 0.65−0.9 nm for $H_2$ adsorption at 77 K.[10] A clear dependence on pore size is found by the relationship between $D_{HK}$ and $H_2$ uptake per SSA (Table 2).[11] The $D_{HK}$ value of the CH35 and CS35 samples is in the optical region of pore size showing high $H_2$ uptake per SSA. Among these samples, CH40 has the highest $S_{BET}$ and $V_t$, but its $H_2$ uptake per SSA is the smallest. It indicates that increasing the mesopore volume ($V_{meso} = V_t - V_{micro}$) is accompanied by a decrease in capacity, and hydrogen storage is dominated by micropores. This is consistent with that reported about dense hydrogen adsorption in subnanometer pores in the literature.[27] Furthermore, it can be concluded that the hydrogen adsorption capability per SSA of the carbon spheres prepared by this template-free method is better than other microporous carbons, and their hydrogen storage is also dominated by small pores (optimal micropore size and volume).

## CONCLUSIONS

A simple and effective template-free method to form micropores in monodisperse carbon spheres and tailor their pore structure has been successfully developed using SPSs or HPCs as the raw materials, anhydrous $AlCl_3$ as the Friedel−Crafts catalyst, and $CCl_4$ as a cross-linker and solvent. The micropore size of the spheres obtained from HPCs increases with sub-angstrom accuracy compared to that of the spheres obtained from SPSs, and their pore volume and SSA change. This is attributed to larger interspaces in h-HCPSs than s-HCPSs and a high cross-linking density provided by the −CO− cross-linking bridges among the P(St-co-DVB) chains. Hydrogen adsorption capability per SSA of the carbon spheres prepared by this template-free method is better than other microporous carbons, and their hydrogen storage is also dominated by small pores (optimal micropore size and volume). Thus, this study supports theoretical predictions that the optimal pore size for hydrogen adsorption should be around 0.65−0.9 nm in carbonaceous adsorbents.

## ASSOCIATED CONTENT

### Supporting Information

SEM photos of SPSs and HPCs samples, TEM photos of s-HCPSs and h-HCPSs samples, XRD patterns of carbon sphere powder samples, Raman spectra of carbon spheres, nitrogen adsorption/desorption isotherms and textural parameters of CH35-900 and CH30, recipes for preparation of core−shell P(St-co-DVB) spheres with different DVB dosage, and materials for synthesis of the samples. This material is available free of charge via the Internet at http://pubs.acs.org.

## AUTHOR INFORMATION

### Corresponding Author

*E-mail: qunxu@zzu.edu.cn.

### Notes

The authors declare no competing financial interest.

## ACKNOWLEDGMENTS

We are grateful for the financial support from the National Natural Science Foundation of China (No. 51202223, 51173170, 21101141, 50955010), Program for Excellent Scientist from Henan province (No.114200510019), and Program for New Century Excellent Talents in University (NCET).

## REFERENCES

(1) Stein, A.; Wang, Z. Y.; Fierke, M. A. Functionalization of porous carbon materials with designed pore architecture. *Adv. Mater.* **2009**, *21*, 265−293.

(2) Drage, T. C.; Snape, C. E.; Stevens, L. A.; Wood, J.; Wang, J. W.; Cooper, A. I.; Dawson, R.; Guo, X.; Satterley, C.; Irons, R. Materials challenges for the development of solid sorbents for post-combustion carbon capture. *J. Mater. Chem.* **2012**, *22*, 2815−2823.

(3) Bo, X. J.; Zhu, L. D.; Wang, G.; Guo, L. P. Template-free synthesis of rectangular mesoporous carbon nanorods and their application as a support for Pt electrocatalysts. *J. Mater. Chem.* **2012**, *22*, 5758−5763.

(4) Chai, S. H.; Howe, J. Y.; Wang, X. Q.; Kidder, M.; Schwartz, V.; Golden, M. L.; Overbury, S. H.; Dai, S.; Jiang, D.-E. Graphitic mesoporous carbon as a support of promoted Rh catalysts for hydrogenation of carbon monoxide to ethanol. *Carbon* **2011**, *50*, 1574−1582.

(5) Jaradat, A. Q.; Grimberg, S. J.; Holsen, T. M.; Ghosh, R. S. Optimum operating conditions for a granular activated carbon filter treating stormwater containing polychlorinated biphenyls: Backwashing and empty bed contact time. *Environ. Eng. Sci.* **2010**, *27*, 403−410.

(6) Merlet, C.; Rotenberg, B.; Madden, P. A.; Taberna, P. L.; Simon, P.; Gogotsi, Y.; Salanne, M. On the molecular origin of supercapacitance in nanoporous carbon electrodes. *Nat. Mater.* **2012**, *11*, 306−310.

(7) Lee, D.; Lee, J.; Kim, J.; Kim, J.; Na, H. B.; Kim, B.; Shin, C.-H.; Kwak, J. H.; Dohnalkova, A.; Grate, J. W.; Hyeon, T.; Kim, H.-S. Simple fabrication of a highly-sensitive and fast glucose biosensor using enzyme immobilized in mesocellular carbon foam. *Adv. Mater.* **2005**, *17*, 2828−2833.

(8) Li, H.; Xi, H. A.; Zhu, S.; Wen, Z.; Wang, R. Preparation, structural characterization, and electrochemical properties of chemically modified mesoporous carbon. *Microporous Mesoporous Mater.* **2006**, *96*, 357−362.

(9) Yushin, G.; Dash, R.; Jagiello, J.; Fischer, J. E.; Gogotsi, Y. Carbide-derived carbons: Effect of pore size on hydrogen uptake and heat of adsorption. *Adv. Funct. Mater.* **2006**, *16*, 2288−2293.

(10) Gigras, A.; Bhatia, S. K.; Anil Kumar, A. V.; Myers, A. L. Feasibility of tailoring for high isosteric heat to improve effectiveness of hydrogen storage in carbons. *Carbon* **2007**, *45*, 1043−1050.

(11) Gogotsi, Y.; Dash, R. K.; Yushin, G.; Yildirim, T.; Laudisio, G.; Fischer, J. E. Tailoring of nanoscale porosity in carbide-derived carbons for hydrogen storage. *J. Am. Chem. Soc.* **2005**, *127*, 16006−16007.

(12) Presser, V.; Heon, M.; Gogotsi, Y. Carbide-derived carbons-from porous networks to nanotubes and graphene. *Adv. Funct. Mater.* **2011**, *21*, 810−833.

(13) Xia, Y.; Yang, Z.; Mokaya, R. Templated nanoscale porous carbons. *Nanoscale* **2010**, *2*, 639−659.

(14) Lee, J.; Kim, J.; Hyeon, T. Recent progress in the synthesis of porous carbon materials. *Adv. Mater.* **2006**, *18*, 2073−2094.

(15) Almasoudi, A.; Mokaya, R. Preparation and hydrogen storage capacity of templated and activated carbons nanocast from commercially available zeolitic imidazolate framework. *J. Mater. Chem.* **2012**, *22*, 146−152.
(16) Xia, Y. D.; Mokaya, R.; Grant, D. M.; Walker, G. S. A simplified synthesis of N-doped zeolite-templated carbons, the control of the level of zeolite-like ordering and its effect on hydrogen storage properties. *Carbon* **2011**, *49*, 844−853.
(17) Yang, Y. X.; Brown, C. M.; Zhao, C. X.; Chaffee, A. L.; Nick, B.; Zhao, D. Y.; Webley, P. A.; Schalch, J.; Simmons, J. M.; Liu, Y.; Her, J.-H.; Buckley, C. E.; Sheppard, D. A. Micro-channel development and hydrogen adsorption properties in templated microporous carbons containing platinum nanoparticles. *Carbon* **2011**, *49*, 1305−1317.
(18) Yang, Z. X.; Xia, Y. D.; Mokaya, R. Enhanced hydrogen storage capacity of high surface area zeolite-like carbon materials. *J. Am. Chem. Soc.* **2007**, *129*, 1673−1679.
(19) Zou, C.; Wu, D. C.; Li, M. Z.; Zeng, Q. C.; Xu, F.; Huang, Z. Y.; Fu, R. W. Template-free fabrication of hierarchical porous carbon by constructing carbonyl crosslinking bridges between polystyrene chains. *J. Mater. Chem.* **2010**, *20*, 731−735.
(20) Yang, Q. Y.; Chen, J. F.; Wang, L. B.; Xu, Q.; He, L. H. Morphology control and 2D self-assembly of poly(styrene-co-divinylbenzene) capsules. *J. Colloid Interface Sci.* **2011**, *358*, 437−443.
(21) Cao, S. S.; Jin, X.; Yuan, X. H.; Wu, W. W.; Hu, J.; Sheng, W. C. A facile method for the preparation of monodisperse hollow silica spheres with controlled shell thickness. *J. Polym. Sci., Part A: Polym. Chem.* **2010**, *48*, 1332−1338.
(22) Li, Y.; Chen, J. F.; Xu, Q.; He, L. H.; Chen, Z. M. Controllable route to solid and hollow monodisperse carbon nanospheres. *J. Phys. Chem. C* **2009**, *113*, 10085−10089.
(23) Kaewtatip, K.; Tanrattanakul, V. Preparation of cassava starch grafted with polystyrene by suspension polymerization. *Carbohydr. Polym.* **2008**, *73*, 647−655.
(24) Hradil, J.; Králová, E. Styrene-divinylbenzene copolymers post-crosslinked with tetrachloromethane. *Polymer* **1998**, *39*, 6041−6048.
(25) Yang, Z.; Xia, Y.; Sun, X.; Mokaya, R. Preparation and hydrogen storage properties of zeolite-templated carbon materials nanocast via chemical vapor deposition: Effect of the zeolite template and nitrogen doping. *J. Phys. Chem. B* **2006**, *110*, 18424−18431.
(26) Jajiello, J.; Ania, C. O.; Parra, J. B.; Jagiello, L.; Pis, J. J. Using DFT analysis of adsorption data of multiple gases including $H_2$ for the comprehensive characterization of microporous carbons. *Carbon* **2007**, *45*, 1066−1071.
(27) Kadono, K.; Kajiura, H.; Shiraishi, M. Dense hydrogen adsorption on carbon subnanopores at 77 K. *Appl. Phys. Lett.* **2003**, *83*, 3392−3394.